On the Assessment of Nonlocal Climate Feedback. Part II: EFA-SVD and Optimal Feedback Modes*

ZHENGYU LIU

Department of Atmospheric and Oceanic Science, Center for Climatic Research, University of Wisconsin—Madison, Madison, Wisconsin

NA WEN

Physical Oceanography Laboratory, The Ocean University of China, Qingdao, China

(Manuscript received 15 May 2007, in final form 9 October 2007)

ABSTRACT

The equilibrium feedback assessment (EFA) is combined with the singular value decomposition (SVD) to assess the large-scale feedback modes from a lower boundary variability field onto an atmospheric field. The leading EFA-SVD modes are the optimal feedback modes, with the lower boundary forcing patterns corresponding to those that generate the largest atmospheric responses, and therefore provide upper bounds of the feedback response. The application of EFA-SVD to an idealized coupled ocean–atmosphere model demonstrates that EFA-SVD is able to extract the leading feedback modes successfully. Furthermore, these large-scale modes are the least sensitive to sampling errors among all the feedback processes and therefore are the most robust for statistical estimation. The EFA-SVD is then applied to the observed North Atlantic ocean–atmosphere system for the assessment of the sea surface temperature (SST) feedback on the surface heat flux and the geopotential height, respectively. The dominant local negative feedback of SST on heat flux is confirmed, with an upper bound of about 40 W m^{-2} K^{-1} for basin-scale anomalies. The SST also seems to exert a strong feedback on the atmospheric geopotential height: the optimal SST forcing has a dipole pattern that generates an optimal response of a North Atlantic Oscillation (NAO) pattern, with an upper bound of about 70 m K^{-1} at 500 hPa. Further issues on the EFA-SVD analysis are also discussed.

1. Introduction

One of the most challenging aspects of the climate system is the interaction between the atmosphere and its lower boundary ocean and land. [Hereafter, the lower boundary will be referred to as the sea surface temperature (SST).] It is well known that the atmosphere exerts a strong control on SST variability. It is also known that the SST variability, in turn, can generate significant feedback response in the atmosphere through local and remote processes. This full climate feedback, however, is difficult to quantify in the observation, or a single realization of a complex coupled ocean–atmosphere model simulation, because of the complex interactions within the climate system, the complex dynamics of climate teleconnection, and the presence of strong internal atmospheric variability. It is clear that a statistical approach is critical, not only for the estimation of the climate feedback in the observation but also for the validation of climate-model feedback and sensitivity. This is because the observation has only a single realization that cannot be repeated, and therefore a statistical estimation approach is the only way to estimate the feedback in the observation. The statistically derived feedback from the observation therefore provides the only parallel comparison between the feedbacks in the model and the observation.

Frankignoul et al. (1998) proposed a simple univariate statistical method, known now as the equilibrium feedback assessment (EFA), for the assessment of climate feedback. This univariate method, in essence, can be used to assess only "local" climate feedback from a single point, or index, of SST variability.

* Center for Climatic Research Contribution Number 928.

Corresponding author address: Z. Liu, CCR, 1225 W. Dayton St., Madison, WI 53706.
E-mail: zliu3@wisc.edu

DOI: 10.1175/2008JCLI2042.1

Recently, Liu et al. (2008, hereafter Part I) proposed a method that is a multivariate generalization of the univariate EFA. This multivariate EFA directly assesses the Green's function of the atmospheric response that is independent of the pattern of SST evolution. Because the Green's function allows for the assessment of the atmospheric response to SST anomaly between any pairs of points or patterns, the EFA estimate, in principle, enables us to assess the full climate feedback, local and nonlocal. Part I demonstrates, indeed, that the multivariate EFA can extract important features of the full climate feedback. However, one major deficiency of the multivariate EFA is the sensitivity to the spatial resolution of the SST forcing field. The sampling error tends to increase significantly with the spatial resolution of SST, except for the cases of very low resolutions. The large sampling error at high resolution occurs because the SST field tends to covary among neighboring regions, leading to a more singular SST covariance matrix and, in turn, a larger sampling error on the EFA estimator.

As a follow-up to Part I, this study is motivated by our speculation that the large-scale feedback process should be less sensitive to resolution and, therefore, more robust for assessment. Here, the large-scale feedback response modes are identified by combining the singular value decomposition (SVD; Bretherton et al. 1992) with the EFA. The leading EFA-SVD modes are found to be the most robust (or least sensitive to resolution) among all the feedback responses. Furthermore, the leading EFA-SVD modes are the optimal feedback modes, in the sense that given amplitude of SST anomaly, the SST-mode patterns generate the greatest atmospheric feedback response. As such, the EFA-SVD analysis provides a useful tool for identifying and understanding large-scale climate feedbacks in the coupled climate system. It should be pointed out that the EFA-SVD differs significantly from the maximum covariance analysis (MCA; Czaja and Frankignoul 2002) in that the latter only seeks the leading SVD modes of the covariance matrix rather than quantifying the feedback response (see appendix A for more discussions on the difference with MCA). This paper is arranged as follows: section 2 introduces the EFA-SVD method. The EFA-SVD is first tested in a simple coupled atmosphere–ocean model in section 3 and is then applied to the observed ocean–atmosphere feedback over the North Atlantic in section 4. A summary is given in section 5.

2. The EFA-SVD analysis

Following Part I, the anomalous fields of atmospheric total variability $\mathbf{x}(t)$, atmospheric internal variability $\mathbf{n}(t)$, and SST variability $\mathbf{y}(t)$ are represented as column vectors

$$\mathbf{x}(t) = \begin{pmatrix} x_1(t) \\ \cdot \\ \cdot \\ \cdot \\ x_I(t) \end{pmatrix}, \quad \mathbf{n}(t) = \begin{pmatrix} n_1(t) \\ \cdot \\ \cdot \\ \cdot \\ n_I(t) \end{pmatrix}, \quad \text{and} \quad \mathbf{y}(t) = \begin{pmatrix} y_1(t) \\ \cdot \\ \cdot \\ \cdot \\ y_J(t) \end{pmatrix},$$

where the atmosphere and SST have I and J points, respectively. The equilibrium atmospheric response at T-succeeding time bins can be rewritten as

$$\mathbf{x}(t) = \mathbf{B}\mathbf{y}(t) + \mathbf{n}(t), \quad t = 1, 2, \ldots, T. \tag{2.1}$$

The length of the time bin, in principle, should be longer than the time scale of the atmospheric internal variability $\mathbf{n}(t)$, such that the equilibrium response (2.1) is approximately valid (after the neglect of the temporal tendency of the atmospheric variability in the atmospheric equations). Hereafter, for simplicity, we have chosen the bin length as 1 month; that is, we use monthly data.

At a lead time τ longer than the persistence time of the atmospheric internal variability, the SST variability $\mathbf{y}(t - \tau)$ is uncorrelated with the internal variability $\mathbf{n}(t)$. Therefore, with right multiplication of $\mathbf{y}(t - \tau)$ on the equilibrium response (2.1), the feedback matrix $\mathbf{B} = {}_I[b_{ij}]_J$ can be estimated in the EFA estimator as (see Part I for details)

$$\mathbf{B}(\tau) = \mathbf{C}_{XY}(\tau)\mathbf{C}_{YY}^{-1}(\tau), \quad \text{for} \quad \tau > 0; \tag{2.2}$$

where

$$\mathbf{C}_{YY}(\tau) = \langle \mathbf{y}(t), \mathbf{y}(t - \tau) \rangle \equiv \frac{1}{T}\mathbf{Y}_t\mathbf{Y}_{t-\tau}^{\mathrm{T}},$$

$$\mathbf{C}_{XY}(\tau) = \langle \mathbf{x}(t), \mathbf{y}(t - \tau) \rangle \equiv \frac{1}{T}\mathbf{X}_t\mathbf{Y}_{t-\tau}^{\mathrm{T}}, \quad \text{and}$$

$$\mathbf{C}_{NY}(\tau) = \langle \mathbf{n}(t), \mathbf{y}(t - \tau) \rangle \equiv \frac{1}{T}\mathbf{N}_t\mathbf{Y}_{t-\tau}^{\mathrm{T}};$$

with the variability matrix as

$$\mathbf{Y}_t = [\mathbf{y}(1), \ldots, \mathbf{y}(T)],$$
$$\mathbf{X}_t = [\mathbf{x}(1), \ldots, \mathbf{x}(T)], \quad \text{and}$$
$$\mathbf{N}_t = [\mathbf{n}(1), \ldots, \mathbf{n}(T)];$$

and the superscript T indicating the transpose. In principle, the EFA estimator (2.2) should be independent of τ for the atmospheric system (2.1), which has a constant matrix $\mathbf{B}$ (as long as τ is longer than the persistence time of the internal variability). In practice, for a given sampling size, a longer τ reduces the SST autocovariance $\mathbf{C}_{YY}(\tau)$ and therefore leads to an increased sampling error in (2.2) [a more detailed discussion is given in Part I for the multivariate case, and in appendix A of Liu et al. (2006) for the univariate case].

Therefore, the rule of thumb is to use a short τ, as long as it is longer than the atmospheric internal variability. For monthly data, τ is usually chosen to be 1–3 months (Frankignoul et al. 1998).

Assuming the rank of $\mathbf{B}$ as $\mathbf{R}$, the SVD decomposition of $\mathbf{B}$ leads to

$$\mathbf{B} = \mathbf{LSR}^{\mathrm{T}} = \sum_{k=1}^{R} s_k \mathbf{l}_k \mathbf{r}_k^{\mathrm{T}}, \tag{2.3}$$

where $\mathbf{L}$ consists of the orthonormal left vectors $\mathbf{l}_i$ for the atmospheric response, $\mathbf{R}$ consists of the orthonormal right vectors $\mathbf{r}_i$ for the SST forcing, and $\mathbf{S}$ is a diagonal matrix with positive singular values in descending order as $s_1 > \ldots > s_i > \ldots s_R > 0$. Right multiplication of (2.3) with $\mathbf{r}_i$ and noticing the orthonormality of $\mathbf{r}_i$ yield

$$s_i \mathbf{l}_i = \mathbf{B}\mathbf{r}_i. \tag{2.4}$$

This can be interpreted, in light of the atmospheric response of Eq. (2.1), as the equilibrium atmospheric response $s_i\mathbf{l}_i$ to the SST forcing $\mathbf{r}_i$. Therefore, ($\mathbf{r}_i$, $\mathbf{l}_i$, s_i) represent the ith optimal feedback modes for a unit magnitude of SST anomaly, with $\mathbf{r}_i$ as the forcing pattern, $\mathbf{l}_i$ as the response pattern, and s_i as the response magnitude. For a finite sample size, the optimal modes can be estimated with the SVD decomposition of the EFA estimator (2.2) of the feedback matrix, with the ith SVD mode as the estimation of the ith optimal feedback mode. In particular, the first SVD mode represents the most optimal feedback mode, with the singular value s_1 as the upper bound for the feedback response under any SST pattern of the same magnitude. Given a general SST anomaly, the atmospheric response can be obtained, in principle, by first projecting the SST anomaly onto all the forcing modes $\{\mathbf{r}_i\}$, and then deriving the corresponding atmospheric response by summing up the responses to each forcing mode in terms of the singular values $\{s_i\}$ and the response mode $\{\mathbf{l}_i\}$ as in Eq. (2.4).

In a climate model, these optimal modes estimated using the statistical method can be checked independently with a dynamical assessment, which uses an ensemble of simulations. For the ith optimal mode, the ensemble experiment will be forced by the ith SST forcing pattern $\mathbf{r}_i$, and then the ensemble atmospheric response will be compared with $\mathbf{l}_i$ for the response pattern, and with s_i for the response magnitude.

3. A simple model study

a. The advective stochastic climate model

As the first illustration, we apply EFA-SVD to the SST feedback on air temperature in a conceptual stochastic climate model that includes nonlocal atmospheric advection. The model is described in detail in Part I and will only be described briefly here for completeness. The coupled model, in the nondimensional form in the model domain $0 \le x \le 1$, consists of the atmospheric equation

$$\partial T_a/\partial x = \lambda(T - T_a) + n(x, t) \tag{3.1}$$

and the oceanic equation

$$\partial T/\partial t = H - dT, \tag{3.2}$$

where T_a is air temperature, T is SST, $H = T_a - T$ is the downward heat flux, and d is the oceanic damping. The relative importance of local coupling versus nonlocal advection is measured by λ, a smaller λ representing a stronger advection or, equivalently, a weaker local coupling.

The atmospheric response to any SST anomaly $\mathbf{T}(t)$ can be obtained by integrating the equilibrium atmospheric Eq. (3.1) downwind along x. After a spatial discretion into I intervals, the atmospheric response can be put in the vector form as (see Part I for more details)

$$\mathbf{T}_a(t) = \mathbf{B}\mathbf{T}(t) + \mathbf{N}(t), \tag{3.3}$$

where

$$\mathbf{T}_a(t) = \begin{pmatrix} T_{a1}(t) \\ \cdot \\ \cdot \\ \cdot \\ T_{aI}(t) \end{pmatrix}, \mathbf{T}(t) = \begin{pmatrix} T_1(t) \\ \cdot \\ \cdot \\ \cdot \\ T_I(t) \end{pmatrix}, \quad \text{and} \quad \mathbf{n}(t) = \begin{pmatrix} n_1(t) \\ \cdot \\ \cdot \\ \cdot \\ n_I(t) \end{pmatrix}.$$

The $\mathbf{N}$ is a transformed stochastic forcing, which can be shown as $\mathbf{N}(t) = (\mathbf{B}/\lambda)\mathbf{n}(t) + T_{a0}(t)\mathbf{q}_b$. Here, the air temperature at the upstream boundary $x = 0$ is $T_{a0}(t)$, which decays downwind following

$$\mathbf{q}_b = \begin{pmatrix} q \\ \cdot \\ \cdot \\ \cdot \\ q^I \end{pmatrix},$$

where $q = e^{-\lambda\Delta x} < 1$. The feedback matrix for T_a can be shown as

$$\mathbf{B} = \lambda\Delta x \begin{bmatrix} 1 & 0 & \dots & 0 \\ q & 1 & \dots & 0 \\ \vdots & \vdots & \dots & \vdots \\ q^{I-1} & q^{I-2} & \dots & 1 \end{bmatrix}. \quad (3.4)$$

This feedback matrix can be interpreted as follows: the positive diagonal elements represent the positive local response of air temperature to SST. The positive off-diagnoal elements represent the nonlocal response, with the ith row representing the response of the air temperature T_{ai} to all the upstream SSTs T_j ($j \le i$), whose influence decays downwind with the distance following an increasing power of q. Alternatively, the jth column represents the remote impacts of the SST forcing T_j on the air temperatures of all downstream points T_{ai} ($i \ge j$), which also decay downwind with the distance.

The coupled system in terms of SST can be obtained by inserting (3.3) into the discretized SST Eq. (3.2) as

$$d\mathbf{T}/dt = (\mathbf{B} - \mathbf{I})\mathbf{T}(t) + \mathbf{N}(t) - d\mathbf{T}, \quad (3.5)$$

where $\lambda\Delta x < 1$ is required for the Courant–Friedrichs–Lewy (CFL) numerical stability criterion.

b. The EFA feedback matrix

We will study the feedback in a 12-point model that is forced by independent stochastic forcings in the interior ($\mathbf{n}$) and the boundary (T_{a0}). With our next application to the observed North Atlantic in mind, a sample size of $T = 500$ will be used. The data are binned in a time interval of 0.5, corresponding roughly to a monthly dataset of 40 yr. We will discuss two cases, a weak advection case and a strong advection case.

For the weak advection case ($\lambda = 4.8$, $d = 0$), the feedback matrix is estimated using the lag-1 EFA estimator (2.2) as $\mathbf{B} = \mathbf{C}_{T_a T}(1)\mathbf{C}_{TT}^{-1}(1)$. To reduce the sampling error, the EFA estimator for each realization is obtained using the leading f SST EOFs as $\mathbf{B}_f$, where $f = 1, 2 \dots 12$ [see Eq. (B.4) of appendix B]. As pointed out in Part I (also appendix B), at a high resolution, a truncation of high-SST EOFs reduces the sampling error by suppressing the singularity of the SST covariance matrix $\mathbf{C}_{TT}$.

The EFA matrix $\mathbf{B}_f$ is compared with the true matrix $\mathbf{B}_{\text{True}}$ [in (3.4)] in terms of its pattern and magnitude, with the pattern measured by the pattern correlation of the two matrices (denoted as $\text{cor}\langle \mathbf{B}_f, \mathbf{B}_{\text{True}} \rangle$) and the magnitude measured in terms of the standard deviations of each matrix as the amplitude ratio $\sigma(\mathbf{B}_f)/\sigma(\mathbf{B}_{\text{True}})$. (Here, the standard deviation is calculated with the elements of the matrix ordered in a single series, and the correlation is calculated between the corresponding elements of the two matrices.) If the two matrices are identical, the correlation and amplitude ratio are both 1. A 1000-member ensemble is performed with the ensemble mean and ensemble spread (one standard deviation of ensemble spread) of the pattern correlation and amplitude ratio plotted in Fig. 1. It is seen that an initial increase of EOF truncation f improves $\mathbf{B}_f$, with an increasing correlation and amplitude ratio toward 1. However, $\mathbf{B}_f$ peaks at the best truncaton $f = 5$ (with a correlation 0.78 and amplitude ratio 0.9). A further increase of f leads to a deteriorated assessment, with a decreased correlation, excessive amplification, and increased ensemble spread. As discussed in Part I, the matrix correlation increases initially due to the increased signal of smaller-scale SSTs, but it decreases eventually because of the increased sampling error associated with high EOFs and, in turn, a singular SST covariance matrix. The amplitude of $\mathbf{B}_f$ always increases with f, because of a more singular $\mathbf{C}_{TT}$.

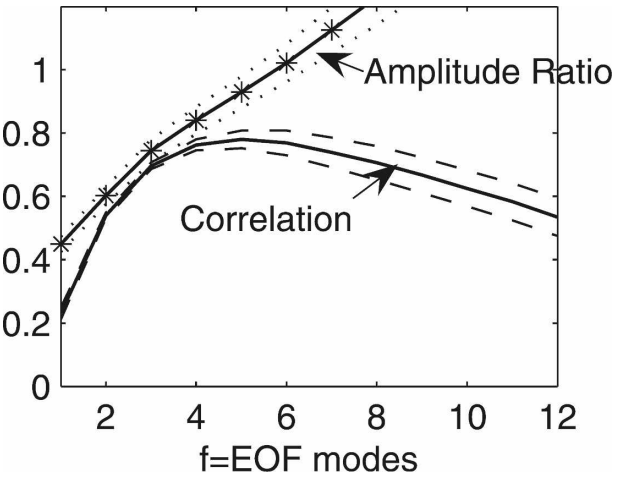

FIG. 1. The EFA feedback matrix in the 12-point model (3.1) and (3.2) for the weak advection case: $\lambda = 4.8$, $d = 0$, $\sigma(n_i) = 10$ ($I = 1, \dots, 12$), and $\sigma(T_{a0}) = 1$. The matrix correlation $\text{cor}\langle \mathbf{B}_f, \mathbf{B}_{\text{True}} \rangle$ (solid line without marker) and amplitude ratio $\sigma(\mathbf{B}_f)/\sigma(\mathbf{B}_{\text{True}})$ between the estimated feedback matrix $\mathbf{B}_f$ and the true feedback matrix $\mathbf{B}_{\text{True}}$ (solid line with asterisks) are shown as functions of the truncation number of SST EOF f. An ensemble of 1000 members are used. The ensemble mean of the matrix correlation is shown by a solid line; the ensemble spread (one std dev) is shown by a dashed line for correlation and a dotted line for amplitude ratio.

Figure 2 shows examples of the feedback matrix for the weak advection case, with the elements. Here, b_{ij} is ordered in a 1D array b_k with $k = i + 12(j - 1)$, increasing first with column j, then with row i. In the true matrix $\mathbf{B}_{\text{True}}$ (solid), the strong local response can be

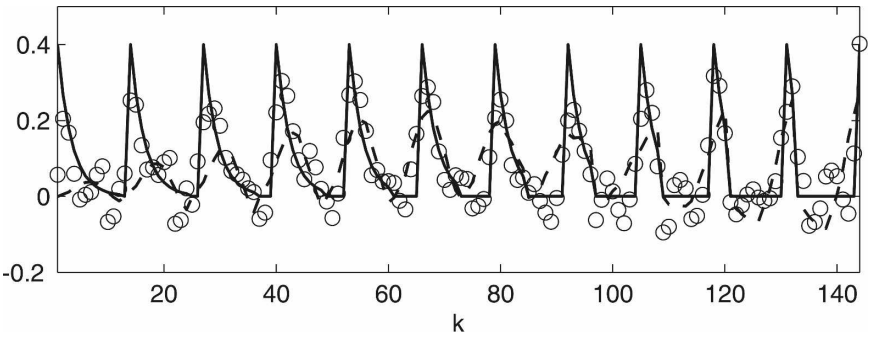

FIG. 2. Examples of the feedback matrix for the weak advection case (in Fig. 1), with the elements b_{ij} arranged along the x axis as b_k in the order of $k = i + 6(j - 1)$. The true feedback matrix $\mathbf{B}$ is shown by a solid line; one ensemble member for $\mathbf{B}_5$ and $\mathbf{B}_2$ is in circles and dashes, respectively.

seen in the positive spikes of the diagonal elements, which according to (3.4) are $b_{jj} = \lambda\Delta x = 0.4$. The positive nonlocal downwind impact is seen as the positive b_k that decreases following each spike because of the decay with distance; the absence of nonlocal impact in the upwind direction is represented by the zeros preceding each spike. Two examples of the EFA estimations are shown, one for $\mathbf{B}_5$ (circles) and the other for $\mathbf{B}_2$ (dash). The $\mathbf{B}_5$ shows modest agreement with $\mathbf{B}_{\text{True}}$, in both the dominant positive local feedback and positive downwind impact. The absence of the upwind impact is also captured by the small values preceding each spike, which are statistically indistinguishable from zero (at the 90% level according to a Monte Carlo test). The $\mathbf{B}_2$ is not as good as $\mathbf{B}_5$ because the former exhibits an excessively smooth large-scale feature. These results are similar to those in Part I.

c. *The EFA-SVD analysis and optimal feedback modes*

Now, we apply SVD to the estimated feedback matrix $\mathbf{B}_f$ to estimate optimal feedback modes. Figure 3a shows SVD1s for each $\mathbf{B}_f$ in comparison with the truth. With EOF1 retained ($\mathbf{B}_1$), SVD1 is poorly estimated, with a mode pattern correlation between the estimated and the true SVD1s as $c^1_{A1} = 0.4$ for the atmospheric response and $c^1_{T1} = 0.43$ for the SST forcing. Here, in c^f_{Am} and c^f_{Tm}, the subscripts A and T stand for the atmospheric response (left) vector and SST forcing (right) vector, respectively, the subscript m stands for the SVD mode number, and the superscript f stands for the SST EOF truncation number. The response amplitude is underestimated by 20% as seen in the ratio of singular values $r^1_1 \equiv s^1_1/s_{1\text{True}} = 0.8$, where the subscript and superscript refer to the SVD mode and EOF truncation, respectively. However, when two EOFs are retained ($\mathbf{B}_2$), SVD1 is improved dramatically, becoming almost perfect ($c^2_{A1} = 0.98$, $c^2_{T1} = 0.93$, and $r^2_1 = 1.0$). The excellent recovery of mode 1 can be seen clearly in Figs. 4a,b, in which the estimated mode 1s (gray) are seen to cluster around the truth (heavy line). Each SVD1 is seen to exhibit a pair of monopoles, and the response is shifted downwind relative to the forcing due to the advection, with the maximum air temperature (at $x = 0.75$) shifted downwind of the maximum SST (at $x = 0.55$) by 0.2.

The successful estimation of optimal feedback mode 1 from the SVD1 of $\mathbf{B}_2$ is in contrast to $\mathbf{B}_2$ itself, which is poorly estimated ($\text{cor}\langle \mathbf{B}_2, \mathbf{B}_{\text{True}} \rangle \sim 0.5$, Fig. 1). One reason for the poor $\mathbf{B}_2$ is that the EOF truncation ($f = 2$) filters out, and therefore distorts, the feedbacks from the SST variability with scales smaller than that of EOF2. Nevertheless, even for the best EFA matrix $\mathbf{B}_5$, the matrix correlation (0.78) and amplitude ratio (0.9) are still substantially lower than the best estimation of the EFA-SVD mode 1 ($c^2_{A1} = 0.98$, $c^2_{T1} = 0.93$, and $r^2_1 = 1.0$). This suggests that mode 1 is estimated more accurately than the feedback matrix itself, with the best estimation obtained at a low EOF truncation of $f = 2$ here. Eventually, however, as more EOFs are included, the estimated SVD1 deteriorates (Fig. 3a), as does the matrix itself (Fig. 1), with a decreased correlation and excessive amplitude. This can be understood as follows: the feedback matrix itself contains the feedback information of all the scales. Feedbacks of smaller scales are likely to be subject to greater sampling errors, because they involve SST variability of stronger neighboring covariability and, in turn, a more singular SST covariance matrix.

The discussion above on mode 1, in principle, applies to other leading modes. This is confirmed for mode 2, which is estimated almost perfectly at $\mathbf{B}_3$ ($c^3_{A2} \approx c^3_{T2} \approx$

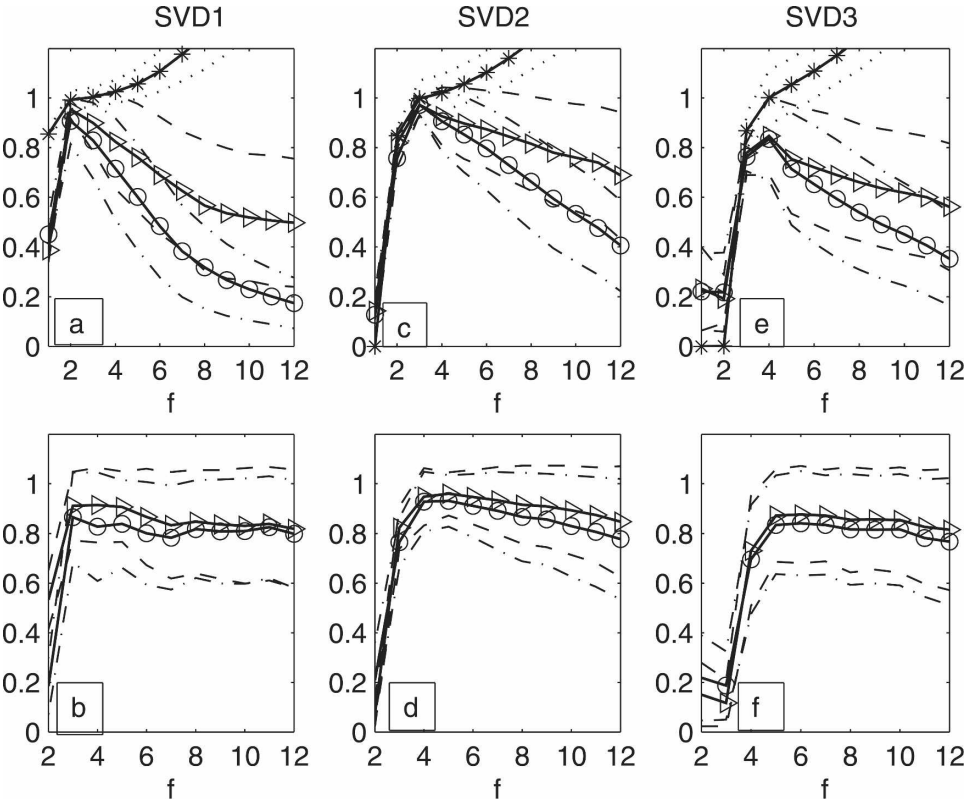

FIG. 3. The optimal feedback modes of the feedback matrix $\mathbf{B}_f$ for the weak advection case in Fig. 1. (a), (b) Mode 1 (SVD1) is shown. (a) Pattern correlations with the truth for the atmospheric response c^f_{A1} (left vector, triangle), SST forcing c^f_{T1} (right vector, circle), and the ratio of the singular values between the estimate and truth r^f_1 (asterisk) as functions of the EOF truncation f. (b) Successive mode pattern correlations for the atmospheric response $c^{f,f-1}_{A1}$ and SST forcing $c^{f,f-1}_{T1}$ as functions of EOF truncation number f. A 1000-member ensemble is used. The ensemble mean is indicated by a solid line, the ensemble spread is indicated by dashes for the atmospheric response correlation, dashes–dots for the SST-forcing correlation, and dots for the amplitude ratio $s^1_1/s_{1\text{True}}$. (c), (d) Same as (a) and (b), respectively, but for mode 2 (SVD2). (e), (f) Same as (a) and (b), respectively, but for mode 3 (SVD3).

$r^3_2 \approx 1$; Fig. 3c), and mode 3, which has the best estimation at $\mathbf{B}_4$ ($c^4_{A3} \approx c^4_{T3} \approx 0.85, r^4_3 \approx 1$; Fig. 3e). The good modal estimation can also be seen clearly in their patterns in Figs. 4c,d for mode 2 and in Figs. 4e,f for mode 3. In both cases, the estimated dipoles (triples) cluster around the truth, and the response shows a downwind shift relative to the forcing. Therefore, all three leading modes can be estimated better than the feedback matrix itself.

The accuracy of all the feedback modes can be seen systematically in Fig. 5a, which shows, for each SVD mode m, the best correlations from the estimations of all of the 12 EOF truncations. As the mode number m increases, the best mode correlations, for both the response and the forcing, decrease initially to about mode 8 and then eventually flatten and increase modestly. The best mode correlations for the first three SVD modes are all higher than the best matrix correlation (dash). In addition, the EOF truncation number f for the best correlation is usually not much larger than the SVD mode number m (Fig. 5b). For example, for SVD mode $m = 1, 2$, and 3, the best correlations are achieved at $f = 2$, 3, and 4, respectively, for both the response and the forcing. This suggests that the leading SVD modes are best obtained without too much smaller-scale SST variability.

The robust estimation of the optimal feedback modes can also be seen in the case of strong advection, which is the same as the weak advection case above, except for an advection 4 times stronger ($\lambda = 1.2$). Now, the true feedback matrix exhibits a much smaller decay downstream (not shown). This feedback matrix is now poorly estimated, with the best matrix correlation of only 0.55 at $\mathbf{B}_2$ with a large spread (Fig. 6). As discussed in Part I, a stronger atmospheric advection forces larger-scale covariance in SST variability, which leads

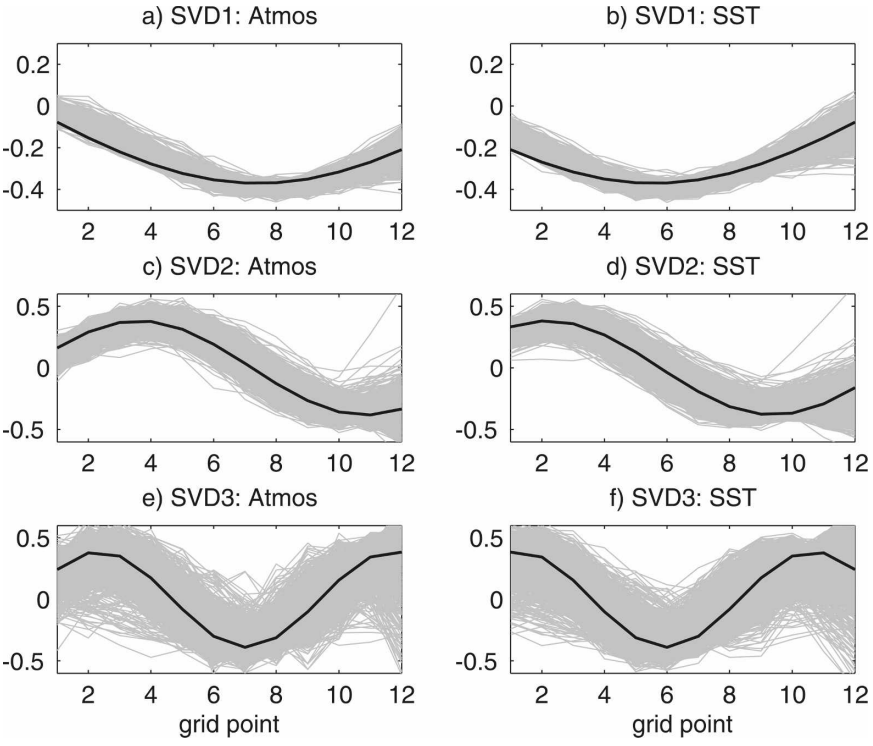

FIG. 4. Patterns of (a) the atmospheric response (left vector) and (b) the SST forcing (right vector) for the best estimate of the optimal mode 1 (SVD1) at the truncation of $f = 2$. The truth is indicated by a heavy solid line and the 1000-ensemble members are indicated by gray lines. (c), (d) Same as (a) and (b), respectively, but for mode 2 at the EOF truncation $f = 3$; (e), (f) Same as (a) and (b), respectively, but for mode 3 at the EOF truncation $f = 4$.

to a more singular SST covariance matrix and, in turn, a greater sampling error. In spite of this poor matrix estimation, the two leading SVD modes can still be estimated rather accurately: mode 1 is best at $\mathbf{B}_2$, with $c_{A1}^2 \approx 0.8$, $c_{T1}^2 \approx 0.82$, and $r_1^2 \approx 1.1$ (Fig. 7a); mode 2 is best at $\mathbf{B}_2$, with $c_{A2}^2 \approx 0.78$, $c_{T2}^2 \approx 0.8$, and $r_2^2 \approx 0.92$ (Fig. 7c), both having a higher correlation than the best matrix correlation (0.55). An examination of the patterns of mode 1 (mode 2) also shows a pair of monopoles (dipoles), with a downwind shift of the response

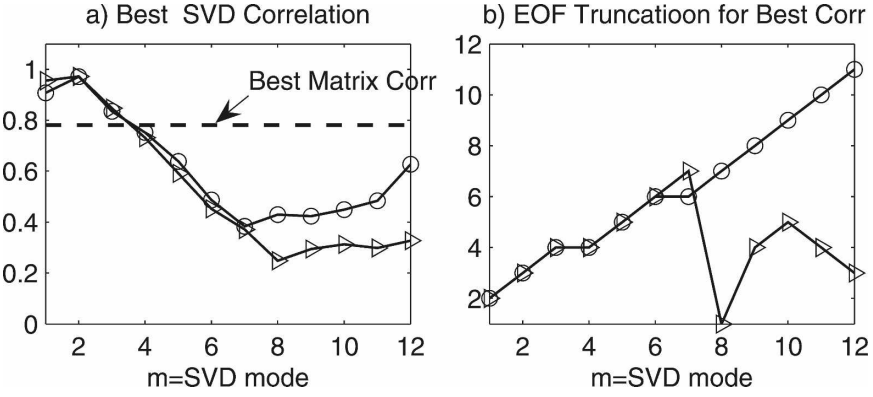

FIG. 5. Best mode correlations for the case of weak advection (in Fig. 1). (a) The best mode pattern correlations with the truth for each optimal feedback mode m. The atmospheric response is shown with triangles and the SST forcing is shown with circles. The best matrix correlation is shown with dashes (for $\mathbf{B}_5$). (b) The EOF truncation f at which the best mode correlations in (a) are achieved.

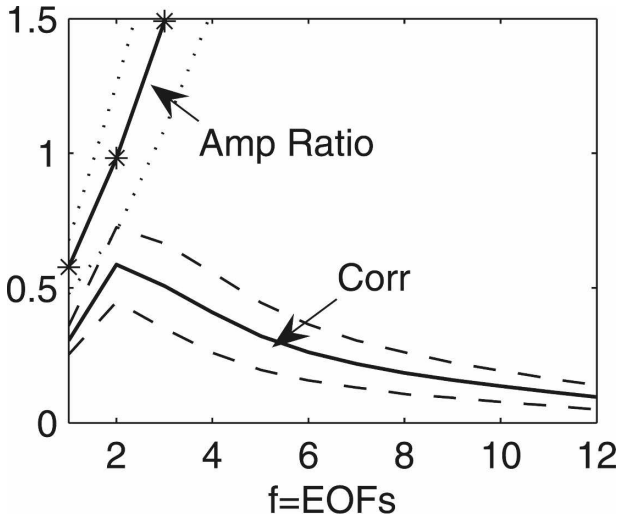

FIG. 6. The EFA feedback matrix as in Fig. 1, but for the case of a strong advection with $\lambda = 1.2$.

more than double that of the weak advection case in Fig. 4 (not shown). Also similar to the weak advection case discussed in Fig. 5, the best mode correlation tends to decrease with the mode number such that they become less than the maximum matrix correlation beyond optimal mode 2 (Fig. 8a); the EOF truncation for the best correlation of the first few leading SVD modes m are not much larger than the SVD mode number f (Fig. 8b).

One advantage of the EFA-SVD analysis, as speculated in the introduction, is the reduction of sensitivity of large-scale feedback processes to the spatial resolution of SST, relative to that for the EFA feedback matrix itself. This is confirmed in the simple model for different resolutions. The leading optimal feedback modes remain robust for different resolutions in both the pattern and amplitude, when the model resolution is doubled and even quadrupled (not shown).

d. The EFA-SVD analysis for a single realization

For the observation (or a complex climate model simulation), the true feedback matrix is unknown and our estimate has to be based on a single realization. This poses a major problem to the EFA-SVD application as to how to determine the best EOF truncation f for each optimal feedback mode m. As in Part I, this best truncation problem remains the major unresolved problem. In the meantime, similar to Part I, our experience with the idealized model suggests an empirical "rule of convergence," which is based on the convergence of the estimated SVD mode m with successive SST EOF truncations. The convergence will be measured by the pattern correlation of the mth SVD modes estimated at the EOF truncations f and f-1, denoted as $c_{Am}^{f,f-1}$ and $c_{Tm}^{f,f-1}$ for the atmosphere and SST, respectively. A visual observation of the convergence for the first three SVD modes in both the weak (Figs. 3b,d,f) and strong (Figs. 7b,d,f) advection cases seems to indicate an approximate rule of convergence, similar to the matrix case discussed in Part I: the best mode correlation is achieved when the mode correlation first converges, that is, at the EOF truncation f beyond which the successive mode correlation ratio plateaus near 1.

Another empirical rule may also be useful. As observed in best mode correlations in Figs. 5b, 8b, the EOF truncation f corresponding to the best mode correlation tends to increase with the optimal mode number m, with best truncation number f slightly exceeding the mode number m. (Although there are occasions when substantially more EOFs are needed for the best correlation of a low-optimal mode.) This implies, perhaps, that to obtain the best estimation of a specific optimal mode, it is necessary to retain at least those SST EOFs that are needed to resolve the optimal modal structure.

The significance of the SVD modes at each EOF truncation can be tested with a Monte Carlo approach similar to the MCA analysis of Czaja and Frankignoul (2002). This significance test will also be seen to help the selection of the best EOF truncation. The Monte Carlo test is illustrated for the case of weak advection (Fig. 3) in Figs. 9a–c. First, one realization of air temperature and SST is selected randomly from those in Fig. 3 as the "observation." Applying the EFA-SVD analysis to the observation leads to the singular values under successive SST EOF truncations as plotted in Figs. 9a–c for SVD1, SVD2, and SVD3, respectively. Second, the observational air temperature is randomly scrambled in time to give an ensemble of 1000 random realizations of the atmosphere. The EFA-SVD is then applied to each random realization of air temperature and the original observational SST to give the spectrum of singular values under each EOF truncation. The ensemble of singular values for SVD1, SVD2, and SVD3 are shown in gray lines in Figs. 9a–c, respectively. The entire ensemble of singular values can be used to construct (one tailed) significance levels (e.g., 95% and 99% levels in heavy dashes in Figs. 9a–c) for testing those observed. The SVD1 is significant at a 99% level for the first four EOF truncations ($f \leq 4$). With a further increase of EOF truncation, the singular value of each random ensemble member continues to increase rapidly, much faster than that of the observation, such that the latter becomes insignificant at a 95% level for

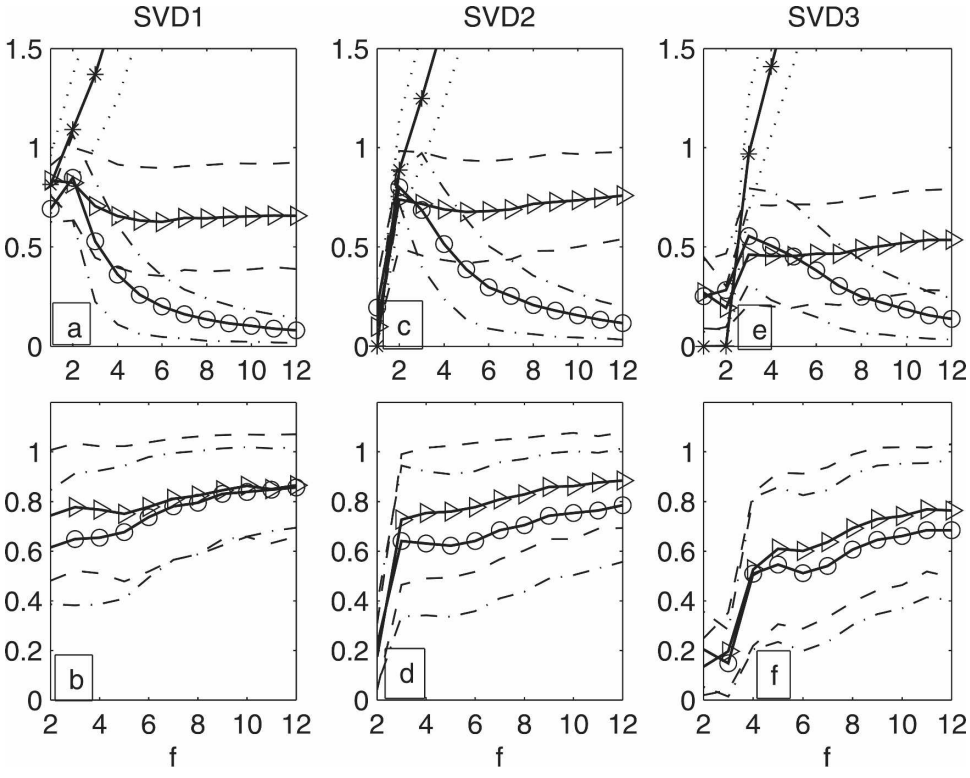

FIG. 7. Correlation and amplitude of the optimal feedback modes as in Fig. 2, but for the case of strong advection in Fig. 6.

EOF truncation beyond $f = 4$. Furthermore, the significance test is consistent with the selection of the best EOF truncation for SVD1 discussed in Fig. 3a, because the best selection of $f = 2$ (see Fig. 3a) is also highly significant in the Monte Carlo test. In addition, the SVD1 is also highly significant for truncations near the best truncation ($f \leq 4$). Therefore, the Monte Carlo test effectively narrows the range for best EOF truncations to a small subset $1 \leq f \leq 4$ that is highly significant for SVD1. In other words, the Monte Carlo test also helps the selection of the best truncation by narrowing down the range of truncation to a small subset. The tests for SVD2 and 3 can be discussed similarly. Now, the singular values are significant at a 99% level for a subset of EOF truncations of $2 \leq f \leq 5$ (Fig. 9b) and $3 \leq f \leq 8$ (Fig. 9c) for SVD2 and 3, respectively. These subsets

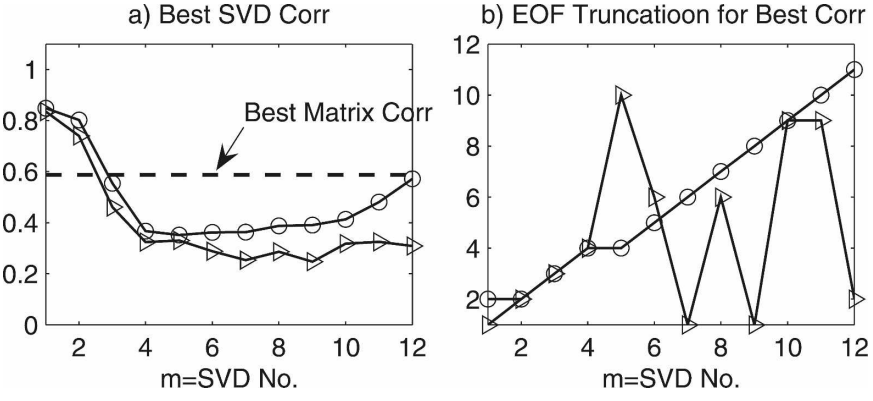

FIG. 8. (a) Best mode correlation and the (b) corresponding EOF truncation as in Fig. 5, but for the case of strong advection in Fig. 6. The best matrix correlation [dashed line in (a)] is now for $\mathbf{B}_2$.

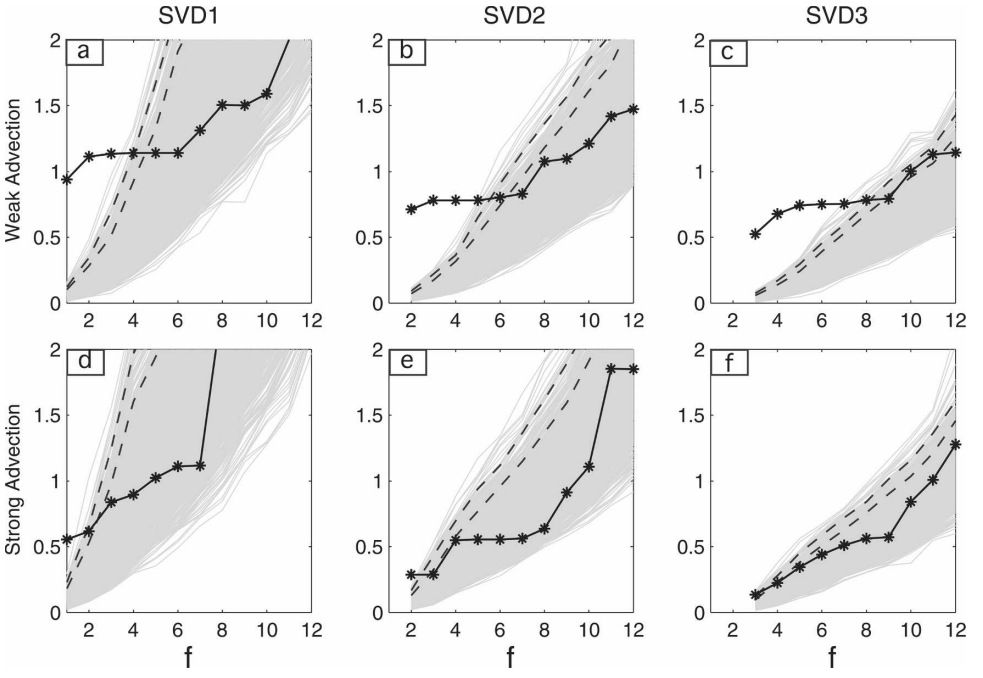

FIG. 9. Monte Carlo test of the singular values of SVD1, SVD2, and SVD3 for the cases of (a)–(c) weak advection (in Fig. 3) and (d)–(f) strong advection (in Fig. 7). In each case, the observation is a single realization randomly selected in Fig. 3 or Fig. 7. (a) Singular values of SVD1 of the observation (asterisk with solid line) for different EOF truncations for the weak advection case. The gray shading is formed by 1000 lines that represent the singular values for the random ensemble of 1000 members, in which the atmosphere is randomly scrambled in time. The 99% and 95% significance levels (one tailed) are marked by heavy dashed lines. (b), (c) Same as (a), but for SVD2 and SVD3. (d)–(f) Same as (a)–(c), respectively, but for the case of strong advection.

clearly include the true best truncations $f = 4$ for both cases (see Figs. 3c,e).

The strong advection case can be discussed similarly (Figs. 9d–f): it has a much smaller range of subset of EOF truncations with significant leading SVDs than does the weak advection case. For example, at the 95% level, the subset of significant EOF truncations is $1 \le f \le 2$, $2 \le f \le 2$, and $3 \le f \le 4$ for SVD1, SVD2, and SVD3, respectively. The much-less-significant singular values overall (relative to the weak advection case) are consistent with the strong noise in the estimation in the strong advection case discussed previously (cf. Figs. 7, 3). Nevertheless, this subset of significant truncations still captures the best truncations of $f = 2$, 2, and 3, for SVD1, SVD2, and SVD3, respectively (see Figs. 7a,c,e). Therefore, in both the weak and strong advection cases, the Monte Carlo test serves dual roles: it provides a significance test for the SVD modes, and it can also help the selection of the best EOF truncations by selecting a subset of significant truncations for a given SVD mode. The latter, combined with the rule of convergence discussed above, can enhance our confidence of the selection of the best EOF truncation significantly.

4. North Atlantic ocean–atmosphere interaction

a. Thermodynamic interaction

We now apply EFA-SVD to study the most optimal feedback mode (mode 1) of ocean–atmosphere interaction over the North Atlantic. Here, we will focus on the application of EFA-SVD, with the details of potential mechanisms left for future studies. The monthly heat flux and SST data are from the Comprehensive Ocean–Atmosphere Data Set (COADS; Woodruff 1985), while the monthly geopotential height is from the National Centers for Environmental Prediction (NCEP) reanalysis, all data in the period of 1957–93. (We also used data entirely from NCEP reanalysis and the results are similar.) All the variables are anomalies from their seasonal cycle; they are area weighted and linearly detrended before the analysis.

As a case of dominant local feedback, we first study the thermal feedback between the SST and the air–sea heat flux (downward positive). It is known that heat flux–SST interaction is dominated by a negative feedback arising from local air–sea interaction. The SST

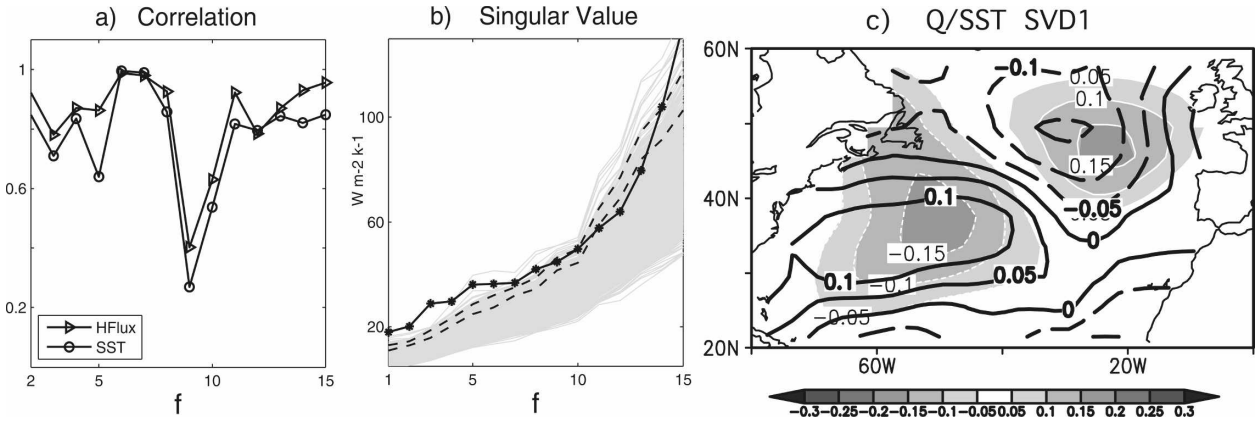

FIG. 10. The most optimal feedback mode (SVD1) for thermal feedback between the SST and surface turbulent heat flux over the North Atlantic. (a) Successive SVD-mode pattern correlations and (b) singular values as functions of the EOF truncation f. In (b), the gray lines indicate those singular values from 1000 random realizations in the Monte Carlo test, and the two heavy dashed lines are the 95% and 99% significance levels. (c) The pattern of the SVD1 of SST (shade) and surface turbulent heat flux (contour) over the North Atlantic selected at $f = 5$. (Positive in solid contours and negative in dashed contours.)

variability is first generated by the atmospheric internal variability and is then damped by the surface turbulent heat flux (Frankignoul et al. 1998), with an upward heat flux response (heat loss) to an SST forcing (warming). This simple damping response provides a clear target to test EFA-SVD in the observation. The area of the North Atlantic (20–60°N, 80°W–0) is divided into ~170 boxes, each 4° × 4°. The EFA-SVD analysis is applied to the heat flux (left) and SST (right) fields. Because the true feedback matrix is unknown, we select the best EOF truncation using our empirical rule of convergence and the Monte Carlo test. Figure 10a shows the successive mode correlations for both the heat flux and SST fields of SVD1 as a function of the truncation f. The mode correlation shows a modest convergence with the correlation peaking around $f = 5$–6 and decreasing sharply beyond $f = 8$. Therefore, the rule of convergence suggests the truncation $f = 5$ (explained SST variance about 60%) as the best truncation for SVD1. This best truncation seems also to be consistent with the convergence of response amplitude (or singular value), which also flattens around $f = 5$ from a small initial increase (Fig. 10b). Furthermore, the Monte Carlo significance test shows that the SVD1 is significant at the 99% level for the subset of truncations of $f \leq 8$, which clearly includes our best truncation $f = 5$.[1] Therefore, the SVD1 at truncation $f = 5$ likely provides a significant true feedback signal in the observation. Figure 10c shows the patterns of mode 1 for the heat flux response (contour) and SST forcing (shading). The SST anomaly is dominated by a dipole in the subtropics and subpolar North Atlantic. These two poles are collocated with the two dominant heat flux centers, with a positive SST forcing an upward heat flux to the atmosphere. This is consistent with the dominantly local negative feedback nature of air–sea thermal feedback. The amplitude of the feedback, at $f = 5$, is about 40 W m^{-2} K^{-1} (Fig. 10b). This feedback magnitude is consistent with the upper bound obtained from local (univariate) EFA feedback analysis for basin-scale anomalies (Frankignoul et al. 1998). The mode patterns of SST forcing and, especially, heat flux response bear a strong resemblance to the EOF1s of SST and heat flux, respectively (not shown). This suggests that the dominant local-feedback mode accounts predominantly for the SST and heat flux variability over the North Atlantic. The estimated mode 1 also remains robust for different resolutions (not shown). This is in contrast to the EFA feedback matrix itself, in which the local-feedback (diagonal) elements become noisy before the resolution is increased beyond 10 boxes (not shown).

The patterns of SVD1s are rather similar from truncation $f = 1$ to 8 (not shown but implied by the successive pattern correlation in Fig. 10a). The major change with the increase of f is the disappearance of a third pole of SST in the tropics (south of 25°N), which was present in the EOF1 of SST as part of the classical tripole SST pattern (not shown). The absence of this tropical SST anomaly pole creates a disparity between SST anomaly and the heat flux there: in spite of the

[1] The best EOF truncation for SVD1 is much higher in the observation than the idealized cases (Figs. 3, 7), because of a much lower explained variance of leading EOFs in the former (17%, 16%, 10%, . . . for EOF1, 2, 3, . . .) than in the latter (65%, 15%, 5%, . . .).

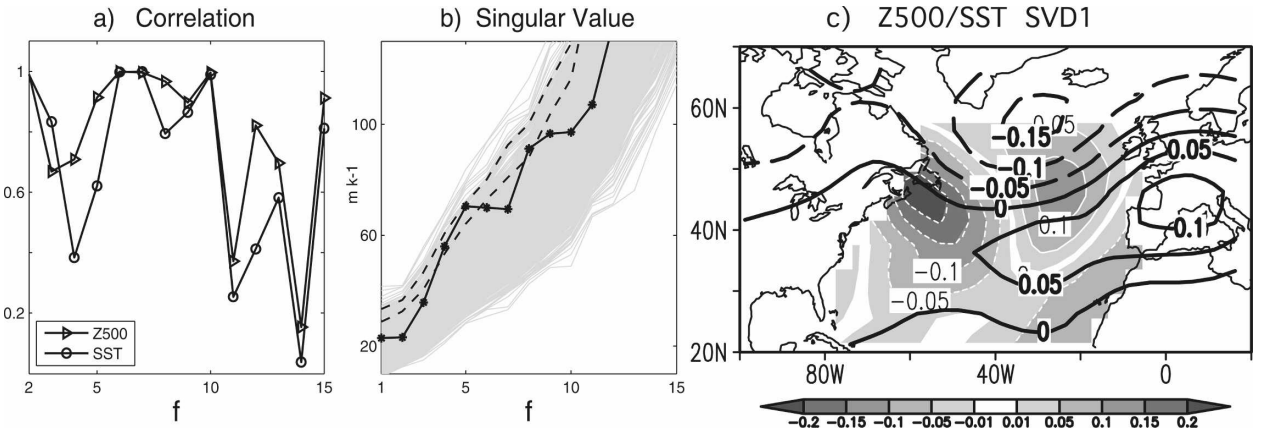

FIG. 11. The optimal feedback mode (SVD1) is the same as Fig. 10, but for the atmospheric dynamic height response at 500 hPa (Z_{500}) to SST over the North Atlantic. (c) This pattern is for EOF of truncation $f = 5$.

absence of an SST anomaly, the heat flux anomaly is modest and of the same sign as that in the subpolar region (Fig. 10c). This heat flux–SST-pattern mismatch may indicate a weak nonlocal heat flux response to SST. A preliminary interpretation of this nonlocal response is associated with a midlatitude SST forcing on the North Atlantic Oscillation (NAO) atmospheric response. The latter is coherent in the tropical and the subpolar North Atlantic and therefore has a nonlocal impact on the tropics. To identify the nonlocal impact unambiguously, one has to assess the feedback matrix itself. A preliminary study of the EFA feedback matrix does indicate some weak nonlocal feedback on tropical heat flux as discussed above. However, the result is significant only for very low resolutions (3–6 boxes, not shown). This example also illustrates one major difficulty for nonlocal feedback assessment: the EFA feedback matrix is good to identify nonlocal feedback, but it is sensitive to resolution. In contrast, the optimal mode identified by EFA-SVD is more robust to resolution, but its low EOF and SVD truncation tends to maintain basin-scale patterns, and it is therefore difficult to isolate a regional forcing effect. One alternative may be to perform the EFA analysis in the space of the leading rotated EOF (as opposed to EOF) of SST (see an example in Zhong and Liu 2008). The rotated EOFs tend to be more localized such that they can be linked to localized regional forcing/response more clearly. In the meantime, the patterns of the leading rotated EOFs, although not perfectly orthogonal as the EOFs are, are usually not highly correlated and therefore should still be effective in reducing the sampling error in the inversion of the SST covariance matrix, similar to the EOFs as discussed in appendix B.

b. *Atmospheric dynamic response*

We now study the SST feedback to the atmospheric geopotential height at 500 hPa (Z_{500}) as a case of strongly nonlocal feedback. In general, atmospheric response to midlatitude SST remains poorly understood (see the review of Kushnir et al. 2002). The mechanism of the atmospheric response is understood to involve nonlinear wave-mean flow interactions (Peng and Whitaker 1999). However, it has remained a great challenge to identify the atmospheric response from the observations, because the strong internal atmospheric variability tends to overwhelm the weak atmospheric response signal. Recently, the EFA (Liu and Wu 2004; Liu et al. 2007) has been used to assess the atmospheric response to extratropical SST anomaly. In spite of the strongly nonlocal nature of atmospheric response, all these applications have used essentially the univariate EFA. It is therefore possible that the atmospheric response is not properly assessed. The MCA analysis (Czaja and Frankignoul 2002), although useful in illustrating the nonlocal nature of the response, does not assess the atmospheric response explicitly (see appendix A). Here, we will use the multivariate EFA-SVD to identify the dominant modes of atmospheric response to North Atlantic SST. The analysis domain is now 20–70°N, 100°W–20°E for the Z_{500}, with ~240 boxes, each 5° × 5°. The SST data are confined to the North Atlantic, the same as the heat flux analysis discussed previously.

The successive mode correlations of Z_{500} and SST for SVD1 suggest that the best truncation for mode 1 is about $f = 5$. This is because the successive mode correlation (Fig. 11a) and the singular value (Fig. 11b) start to plateau at $f = 4$–5. Furthermore, the Monte Carlo

test shows that $f = 5$ is the only truncation that shows significant SVD1 at the 99% level (Fig. 11b).[2] The pattern of mode 1 (Fig. 11c) shows roughly a north–south dipole in SST within the Atlantic basin and a north–south dipole in Z_{500}, both between the subtropical and subpolar regions. The sign is such that a cold SST in the Gulf Stream region generates a low in the Iceland Low. This is consistent with more recent high-resolution atmospheric model simulations (Kushnir et al. 2002). Some longitude variations are also apparent here, with the south pole of SST weakest in the central ocean and the south pole of Z_{500} shifted eastward toward southern Europe. The dipole SST pattern is rather stable from $f = 4$–9 (not shown but implied in the correlation in Fig. 11a), which originates from an initial tripole pattern at $f = 1$ in EOF1 of SST with the southern pole vanishing at $f = 4$. The dipole Z_{500} pattern is also stable between $f = 4$–9, somewhat resembling the NAO pattern as derived from the EOF1 of Z_{500}.[3] Initially at $f = 1$, the Z_{500} pattern exhibits a zonal tripole centered along 50°N, which collapses quickly to a meridional dipole after f increases beyond 3. The magnitude of the response is 70 m K^{-1} at $f = 5$ (Fig. 11b), which seems to be consistent with previous works as being an upper bound of the atmospheric response (Czaja and Frankignoul 2002; Liu and Wu 2004; Liu et al. 2007).

This optimal dipole SST forcing has not been identified in previous work. In a recent MCA analysis, Czaja and Frankigoul (2002) identified a horseshoe pattern of later summer SST forcing early winter NAO. The horseshoe SST pattern differs from the dipole here mainly in the southern pole in the tropics. This difference may be due to the different seasonality between the two analyses. More importantly, the optimal mode identified here does not represent the dominant MCA mode in the couple system (see appendix A). It is also possible that the horseshoe pattern is distorted by the tropical Atlantic forcing (Peng et al. 2005). The identified optimal feedback mode may have implications for ocean–atmosphere coupling over the North Atlantic. The NAO atmospheric variability tends to force a triple SST anomaly through mainly the turbulent heat fluxes (Cayan 1992), and this tripole SST anomaly is the dominant EOF mode for SST over the North Atlantic. It is therefore interesting that the NAO atmospheric response is optimal to a dipole SST forcing, instead of the tripole SST. If true, it implies that the coupling between the atmosphere and SST in the North Atlantic may not form a simple stationary feedback. Instead, some phase shifting will be involved. All these issues remain to be studied in the future.

5. Summary

As an extension of Part I, the SVD decomposition is used on the EFA estimator of the feedback matrix. This EFA-SVD analysis identifies robust large-scale feedback modes with the greatest feedback responses. An application to a simple coupled model suggests that EFA-SVD is able to estimate large-scale, optimal feedback modes more accurately than the smaller-scale feedback modes and, in turn, the overall feedback matrix itself. This suggests that large-scale optimal modes are more robust to the resolutions than the overall feedback matrix itself. The EFA-SVD is then applied to the observed North Atlantic to study ocean–atmosphere feedbacks. The application to the North Atlantic thermal feedback confirms the strong local negative feedback of SST on heat flux with an upper bound of ~40 W m^{-2} K^{-1}. The application to the North Atlantic atmospheric geopotential height response identified a strong NAO response to a North Atlantic dipole SST, with an upper bound of ~70 m K^{-1} for Z_{500}.

As in the case of the feedback matrix in Part I, it remains an issue how to select the best estimator for the optimal feedback modes, especially the best truncation of SST EOFs. The essence of the sampling error with resolution is the covariability of SST among different regions. Both the SST EOF truncation and the SVD decomposition are used to constrain the scales of the feedback fields and therefore constrain the sampling error. So far, this constraint is somewhat ad hoc and subjective. Nevertheless, our empirical rule of convergence, when combined with the Monte Carlo test, seems to be rather effective in selecting the best truncation of EOF. Ultimately, it is highly desirable to develop an assessment method that can take into account the SST spatial correlation objectively. It is also important to better understand the physical mechanism for the identified feedback-response modes, preferably with direct dynamic modeling simulations in climate models.

Acknowledgments. This work is supported by DOE, NOAA, Chinese NSF, and the Ocean University of China. We thank three anonymous reviewers and Dr.

[2] The SVD2 and SVD3 are no longer significant at a 95% level for $Z_{500,}$ but they are still significant for heat flux (not shown). The high SVDs for the heat flux/SST still show a dominant local response but with some interesting phase shifts. These will not be discussed here.

[3] Different from the classical NAO, which is derived from the winter months, the Z_{500} pattern in Fig. 11c is derived for yearround.

D. Straus, whose comments have helped improve the manuscript significantly.

APPENDIX A

EFA-SVD and MCA

In an attempt to identify the full climate feedback, including local and nonlocal responses, Czaja and Frankignoul (2002) used MCA to identify the leading coupled ocean–atmosphere modes, with the patterns of the leading pairs of the response and forcing as the leading pairs of the SVD modes of the covariance matrix $\mathbf{C}_{XY}(\tau)$ between the atmospheric response field (left field) and the SST forcing field of an earlier time (right field). Note, however, that these leading MCA modes depend not only on the atmospheric response sensitivity but also on the SST variability, because the covariance matrix depends on the SST variability in the coupled system as well as on the atmospheric variability. Therefore, the MCA modes mix the atmospheric response with the SST variability in the coupled system. In comparison, the EFA-SVD modes are the SVD decomposition of $\mathbf{C}_{XY}(\tau)\mathbf{C}_{YY}^{-1}(\tau)$, which is a statistical estimator of the feedback matrix $\mathbf{B}$ as shown in (2.2). The former is specific to the coupled system because the SST variability is determined by the coupled system, while the latter depends only on the atmospheric dynamics. Furthermore, given an SST anomaly field in general, the atmospheric response can be predicted directly by the projection of the SST onto the EFA-SVD SST modes, but the atmospheric response cannot be predicted by the projection onto the MCA SST modes. Finally, even if an SST anomaly has the pattern as, say, the SST pattern of the first MCA SST mode, the correspoinding first atmospheric mode only represents the pattern that has the largest covariance with the SST rather than the true atmospheric response pattern to this SST anomaly. In spite of all the desirable advantages of the EFA-SVD, for a finite sample size, the EFA-SVD is much more sensitive to estimation than the MCA, because the MCA does not involve the inverse of the SST covariance matrix as in the EFA estimator (2.2).

APPENDIX B

EFA in the EOF Space

EFA can be performed in the EOF space or subspace. In general, the atmospheric field $\mathbf{x}(t)$ and SST field $\mathbf{y}(t)$ can be expanded on their EOF subspaces as $\hat{\mathbf{x}}(t) = \sum_{i=1}^{\hat{I}} p_i(t)\mathbf{e}_i$ and $\hat{\mathbf{y}}(t) = \sum_{j=1}^{\hat{J}} q_j(t)\mathbf{f}_j$, where $\mathbf{e}_i$ and $\mathbf{f}_j$ are the orthonormal EOFs, $p_i(t) = \mathbf{e}_i^{\mathrm{T}}\mathbf{x}(t)$ and $q_j(t) = \mathbf{f}_j^{\mathrm{T}}\mathbf{y}(t)$ are the corresponding principal components (PCs), and $\hat{I} \le I$ and $\hat{J} \le J$ represent the number of EOFs in the subspaces. Define the EOF and PC matrices as $\mathbf{E} = {}_I[\mathbf{e}_1, \ldots, \mathbf{e}_{\hat{I}}]_{\hat{I}}$, $\mathbf{F} = {}_J[\mathbf{f}_1, \ldots, \mathbf{f}_{\hat{J}}]_{\hat{J}}$, and $\mathbf{P}_t = {}_{\hat{I}}[\mathbf{p}_i(t)]_T$, $\mathbf{Q}_t = {}_{\hat{J}}[\mathbf{q}_j(t)]_T$. The synthetic atmospheric and SST matrices are

$$\hat{\mathbf{X}}_t = \mathbf{E}\mathbf{P}_t \quad \text{and} \quad \hat{\mathbf{Y}}_t = \mathbf{F}\mathbf{Q}_t. \tag{B.1}$$

The equilibrium atmospheric response (2.1) is therefore

$$\hat{\mathbf{X}}_t = \mathbf{B}\hat{\mathbf{Y}}_t + \hat{\mathbf{N}}_t,$$

Substituting in (B.1), and with the orthonormal condition $\mathbf{E}^{\mathrm{T}}\mathbf{E} = \mathbf{I}$, we have

$$\mathbf{P}_t = \mathbf{B}_{\mathrm{EOF}}\mathbf{Q}_t + \mathbf{N}_{\mathrm{EOF}},$$

where

$$\mathbf{B}_{\mathrm{EOF}} = \mathbf{E}^{\mathrm{T}}\mathbf{B}\mathbf{F} \tag{B.2}$$

is the feedback matrix in the EOF subspaces and $\mathbf{N}_{\mathrm{EOF}} = \mathbf{E}^{\mathrm{T}}\hat{\mathbf{N}}_t$ is the internal variability projection on the EOF space. Right multiplication of $\mathbf{Q}_{t-\tau}^{\mathrm{T}}$ and ensemble averaging yield

$$\mathbf{B}_{\mathrm{EOF}} = \mathbf{C}_{PQ}(\tau)\mathbf{C}_{QQ}^{-1}(\tau), \tag{B.3}$$

where we have used $\langle \hat{\mathbf{N}}_t, \mathbf{Q}_{t-\tau} \rangle = 0$. Using (B.2) and the orthonormal condition $\mathbf{F}^{\mathrm{T}}\mathbf{F} = \mathbf{I}$, we recover the feedback matrix in the physical space reconstructed from the EOF subspace of the leading $\hat{I}$ atmospheric and $\hat{J}$ SST EOFs as

$$\mathbf{B}_{\hat{I},\hat{J}} = \mathbf{E}\mathbf{B}_{\mathrm{EOF}}\mathbf{F}^{\mathrm{T}}. \tag{B.4}$$

Notice that the truncation of the SST EOF subspace makes $\mathbf{C}_{QQ}(\tau)$ less singular at small lags. Indeed, at lag 0, we have from the orthorgonality of the PCs

$$\mathbf{C}_{QQ}(0) = \mathbf{Q}^{\mathrm{T}}\mathbf{Q} = \begin{bmatrix} \lambda_1 & 0 & 0 \\ 0 & \cdots & 0 \\ 0 & 0 & \lambda_{\hat{J}} \end{bmatrix},$$

where λ_j is the jth leading eigenvalue of $\mathbf{C}_{YY}(0)$. Therefore, $\mathbf{C}_{QQ}(0)$ will no longer be singular if high SST EOFs of nearly zero eigenvalues are neglected. Furthermore, since SST usually has a long persistence time, we would expect $\mathbf{C}_{QQ}(\tau)$ to be similar to $\mathbf{C}_{QQ}(0)$ at small lags, being not very singular. Therefore, the sampling error of the estimation is reduced in the subspace of SST EOFs in (B.3). It should also be noted that to reduce the sampling error, we only need to reduce the singularity of the SST field, not the atmospheric field. Therefore, in Part I and herein, we only applied the EOF truncation to the SST field.

REFERENCES

Bretherton, C., C. Smith, and J. M. Wallace, 1992: An intercomparison of methods for finding coupled patterns in climate data. *J. Climate,* **5,** 541–560.

Cayan, D., 1992: Latent and sensible heat flux anomalies over the northern oceans: Driving the sea surface temperature. *J. Phys. Oceanogr.,* **22,** 859–881.

Czaja, A., and C. Frankignoul, 2002: Observed impact of North Atlantic SST anomalies on the North Atlantic Oscillation. *J. Climate,* **15,** 606–623.

Frankignoul, C., A. Czaja, and B. L'Heveder, 1998: Air–sea feedback in the North Atlantic and surface boundary conditions for ocean models. *J. Climate,* **11,** 2310–2324.

Kushnir, Y., W. A. Robinson, I. Blade, N. M. J. Hall, S. Peng, and R. Sutton, 2002: Atmospheric GCM response to extratropical SST anomalies: Synthesis and evaluation. *J. Climate,* **15,** 2233–2256.

Liu, Z., and L. Wu, 2004: Atmospheric response to North Pacific SST: The role of ocean–atmosphere coupling. *J. Climate,* **17,** 1859–1882.

——, M. Notaro, J. Kutzbach, and N. Liu, 2006: Assessing climate-vegetation feedback from the observation: The global analysis. *J. Climate,* **19,** 787–814.

——, Y. Liu, L. Wu, and R. Jacob, 2007: Seasonal and long-term atmospheric response to reemerging North Pacific Ocean variability: A combined dynamical and statistical assessment. *J. Climate,* **20,** 955–980.

——, N. Wen, and Y. Liu, 2008: On the assessment of nonlocal climate feedback. Part I: The generalized equilibrium feedback assessment. *J. Climate,* **21,** 134–148.

Peng, S., and J. S. Whitaker, 1999: Mechanisms determining the atmospheric response to midlatitude SST anomalies. *J. Climate,* **12,** 1393–1408.

——, W. A. Robinson, S. Li, and M. P. Hoerling, 2005: Tropical Atlantic SST forcing of coupled North Atlantic seasonal responses. *J. Climate,* **18,** 480–496.

Woodruff, S. D., 1985: COADS Release 2. *Phys. Chem. Earth,* **23,** 517–527.

Zhong, Y. F., and Z. Liu, 2008: A joint statistical and dynamical assessment of atmospheric response to North Pacific oceanic variability in CCSM3. *J. Climate,* in press.